# Electromagnetic Saturation of Angstrom-Sized Quantum Barriers at Terahertz Frequencies

Young-Mi Bahk,[1] Bong Joo Kang,[2] Yong Seung Kim,[3] Joon-Yeon Kim,[1] Won Tae Kim,[2] Tae Yun Kim,[4] Taehee Kang,[1] Jiyeah Rhie,[1] Sanghoon Han,[5] Cheol-Hwan Park,[4] Fabian Rotermund,[2,*] and Dai-Sik Kim[1,†]

[1]*Department of Physics and Astronomy and Center for Atomic Scale Electromagnetism, Seoul National University, Seoul 151-747, Korea*

[2]*Department of Energy Systems Research and Department of Physics, Ajou University, Suwon 443-749, Korea*

[3]*Graphene Research Institute and Department of Physics, Sejong University, Seoul 143-747, Korea*

[4]*Department of Physics and Astronomy and Center for Theoretical Physics, Seoul National University, Seoul 151-747, Korea*

[5]*Photonic Systems Laboratory, School of EECS, Seoul National University, Seoul 151-744, Korea*

(Received 26 March 2015; published 16 September 2015)

Metal-graphene-metal hybrid structures allow angstrom-scale van der Waals gaps, across which electron tunneling occurs. We squeeze terahertz electromagnetic waves through these $\lambda/10\,000\,000$ gaps, accompanied by giant field enhancements. Unprecedented transmission reduction of 97% is achieved with the transient voltage across the gap saturating at 5 V. Electron tunneling facilitated by the transient electric field strongly modifies the gap index, starting a self-limiting process related to the barrier height. Our work enables greater interplay between classical optics and quantum tunneling, and provides optical indices to the van der Waals gaps.

DOI: 10.1103/PhysRevLett.115.125501 PACS numbers: 81.05.ue, 42.50.-p, 42.65.-k

Since the discovery of two-dimensional (2D) crystal layers such as graphene, hexagonal boron nitride (hBN), and molybdenum disulphide ($MoS_2$), there has been intense research on van der Waals (vdW) heterostructures, made by stacking various 2D layers [1,2]. The diversity of atomically thin materials and their heterostructures opens the possibility of new electrical and optical properties as well as novel physical phenomena and device functionalities at the angstrom scale: van der Waals epitaxy [3]; band gap engineering [4]; high-$T_C$ superconductivity [5–7]; room-temperature excitonic superfluidity [8,9]. The interfaces in various vdW heterostructures are found to be clean and atomically sharp because vdW bondings are weak [3], which opens a new possibility of angstrom-gap lithography.

Figure 1 (top) shows a cross-sectional TEM image and vertically averaged line profile of a metal (copper)-single layer graphene (SLG)-metal (copper) structure where two bright lines, each with a width of about 1.5 Å, are clearly seen. These lines indicate the double vdW gaps with generally low electron density, formed between the graphene layer and the surrounding copper surfaces. The red curve (middle) shows the plane-averaged inverse valence electron charge density obtained from density functional theory calculations, in agreement with the 1.5 Å-wide double-gap picture. These gaps with a single layer of carbon atoms in the middle have been approximated by a single 3-Å-wide gap of permittivity three [10,11] (bottom), across which quantum tunneling may occur [11–14].

To study the angstrom gap using visible or infrared light is not a trivial task, because the wavelength is several orders of magnitude longer than the gap width. For exclusive probing and manipulation, it behooves all the incoming electromagnetic waves to squeeze through the angstrom gap without any strays. A metallic nanogap at longer

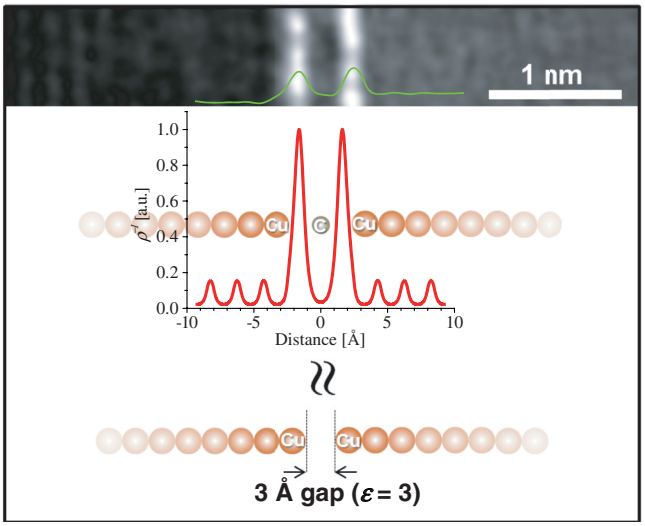


FIG. 1 (color). (Top) Cross-sectional TEM image and vertically averaged line profile of copper (Cu)-single layer graphene (SLG)-Cu composite. SLG was grown on 300-nm-thick Cu film by chemical vapor deposition (CVD). Two bright lines with an average thickness of ~1.5 Å are clearly visible at Cu-SLG-Cu interfaces, indicative of two van der Waals gaps. (Middle) The plotted red curve denotes the plane-averaged inverse valence electron charge density through a line of Cu-carbon-Cu atoms calculated by density functional theory. (Bottom) The graphene spacer with double angstrom gaps is approximated by a single 3-Å-wide gap with permittivity of three.

 

wavelengths naturally accompanies gigantic field enhancement [15–21], allowing exclusive probing of the gap itself. In particular, to see only the angstrom gaps without the usual background optical signals, for ready comparison with theory one is required to manufacture ultralong angstrom gaps much longer than any of the wavelengths of the incoming light used in experiments. In this Letter, for exclusive, background-free probing of the quantum barrier using electromagnetic waves, we manufactured angstrom-sized gaps of 5 mm length, through which virtually all terahertz (THz) waves funnel. To our surprise, record nonlinearity, far greater than its optical counterparts, is found, which enables determination of both the effective barrier height and effective width. Our work has far reaching implications towards vdW gap masks for angstrom lithography, as well as in the emerging field of long wavelength quantum plasmonics.

The angstrom gaps are made as follows [see Fig. 2(a)]. First, we patterned a 300-nm-thick copper (Cu) film with a desired array of rectangular structure of 5 mm by 0.2 mm onto a quartz substrate using the standard photolithography technique. An SLG was then seamlessly grown on the patterned Cu layer also covering the sidewalls. For the graphene growth, a flowing mixture of methane and hydrogen gases were used in a chemical vapor deposition (CVD) system, where the pressure was kept at 10 mTorr. After growing graphene directly on the patterned Cu film, a thinner secondary Cu layer was additionally deposited on the same sample by thermal evaporation filling the trench. Finally, adhesive tape was applied to the surface to peel off the second Cu layer selectively. The resulting final Cu-SLG-Cu composite sample is shown in Fig. 2(b). Figure 2(c) shows top views of the SEM (left), reflection type (center), and dark field scattering (right) optical microscope images of the sample used in our experiments. With the THz spot size of about 2.5 mm, the structure can be considered as an array of *infinitely* long slits with a period of 0.2 mm, for the most frequencies used.

We performed THz time-domain spectroscopy using both an oscillator- and amplifier-based THz system [22]. A femtosecond Ti:sapphire laser operating at an 80-MHz repetition rate is used to illuminate a biased GaAs emitter for generation of single-cycle THz pulses with peak electric field of 30 V/cm at the focus. In addition, we employed pulse-front-tilted efficient optical rectification in a prism-cut $LiNbO_3$ crystal based on a 1-kHz Ti:sapphire regenerative amplifier system for intense THz wave generation [26]. The maximum incident electric field is 200 kV/cm at the focus. The strength of the THz electric field can be varied with a pair of wire grid polarizers, allowing us to change the field amplitude from 10 to 200 kV/cm. In both setups, the transmitted THz field amplitudes are collected with parabolic mirrors and detected by electro-optic sampling technique using $\langle 110 \rangle$ oriented ZnTe and GaP crystals.

Figure 3(a) shows measured time traces of THz field amplitudes transmitted through the sample for various

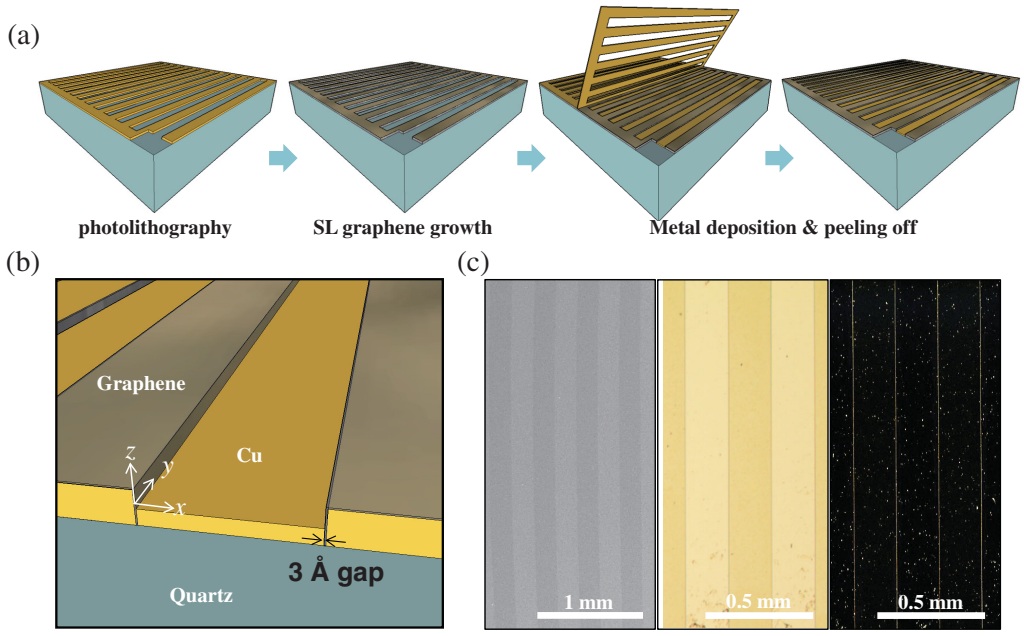


FIG. 2 (color). (a) Schematic of fabrication procedure for vertically oriented graphene spacer in Cu-SLG-Cu composite. First, a patterned Cu layer with desired geometry is prepared by photolithography. Subsequently, SLG is directly grown on the patterned Cu layer by the CVD method. The second Cu layer is then deposited over the graphene-deposited patterned Cu film and an adhesive tape is applied to the surface to peel off the second Cu layer selectively. (b) Cross-sectional view of Cu-SLG-Cu composite array. An SLG spacer forms vertically oriented angstrom gaps through which normally incident THz waves squeeze. (c) Top views of SEM (left), reflection type (center), and dark field scattering (right) optical microscope images of the Cu-SLG-Cu sample used in our experiment.

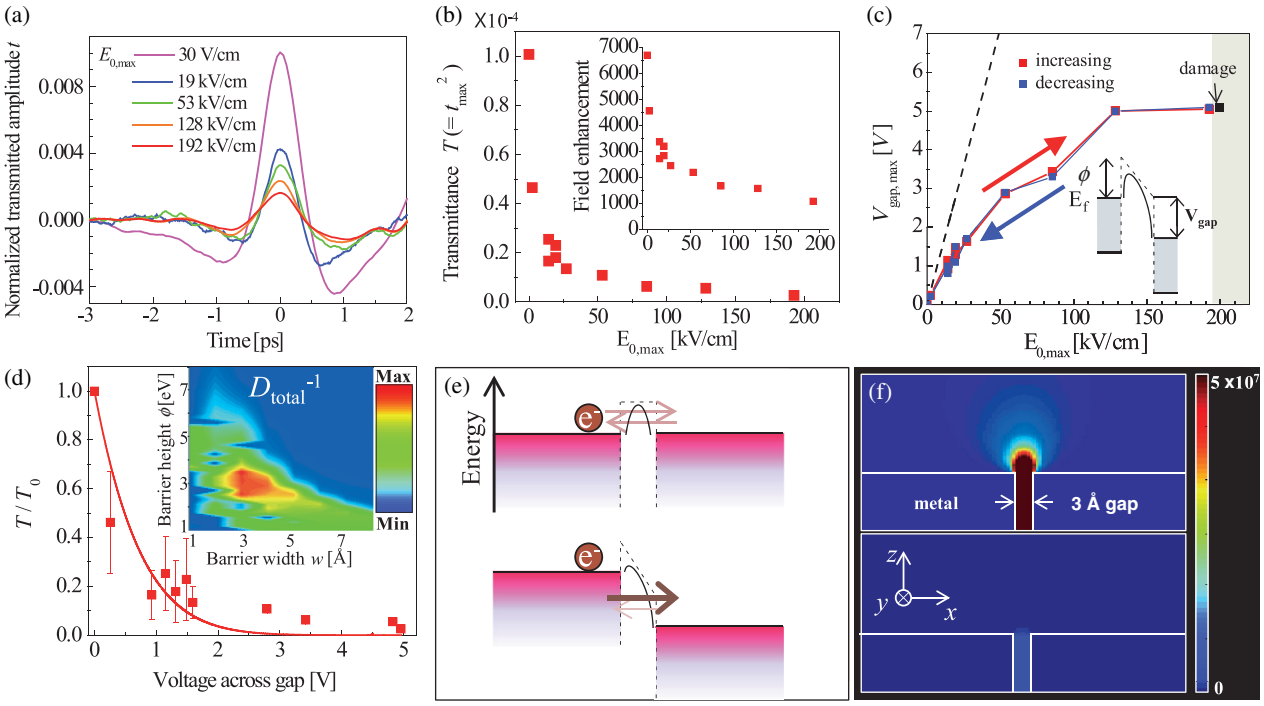


FIG. 3 (color). (a) Time traces of transmitted THz electric field through the Cu-SLG-Cu sample normalized by the substrate transmission for various THz field strengths. (b) Maximum normalized transmittance as a function of the incident THz electric field. Inset: Maximum field enhancement vs the incident electric field. (c) Transient voltage across the gap as we increase (red dot) and then decrease (blue dot) the incident THz electric field. Note that the nonlinear response is reproducible as long as the incident THz field stays below the breakdown field of 200 kV/cm. The dotted line is the case without nonlinearity assuming the same field enhancement for all field strengths. (d) Experimental and calculated nonlinear optical response $T/T_0$ of the SLG-based angstrom gap sample as a function of the applied bias voltage for $w = 3$ Å and $\phi = 3$ eV. $T_0$ is the transmittance in the linear regime. Inset: The inverse of the total sum of the square of the difference between the calculation and the experimental data for various barrier heights $\phi$ and widths $w$. (e) Tunneling barrier profiles in the angstrom gaps for the low (top) and high (bottom) voltages across the gap. (f) Calculated normalized intensity distribution near the 3-Å-wide gap for low-(top) and high-field (bottom) cases.

incident THz pulse strengths, divided by the maximum field amplitudes transmitted through the quartz-substrate only. For low-intensity THz pulses generated with an oscillator-based setup ($E_{0,\max} \sim 30$ V/cm), the normalized amplitude $t$ after subtracting direct transmission (~0.15%) is about 1.0% at the maximum of the single-cycle pulse in the time domain. This one percent transmission is in fact extremely high, when one considers the gap size $w$ of only 3 Å [11], so that the coverage ratio is extremely small: $\beta = w/d = 3$ Å$/0.2$ mm $= 1.5 \times 10^{-6}$, where $d$ is the period. Thereby, a field enhancement of $t/\beta \sim 7000$ is extracted by the Kirchhoff integral formalism [17,31–33]. The measured huge field enhancement, even larger than those achieved with the help of resonance for 1 nm gap rings [34], is a clear evidence for the formation of an effective gap of subnanometer width by the metal-graphene-metal configuration [11,35,36]. This is consistent with the nonmetallic behavior of graphene with respect to the external electric field perpendicular to the surface [10].

As we increase the incident THz electric field up to $E_{0,\max} \sim 192$ kV/cm, the normalized transmitted amplitude in the time domain dramatically decreases, down to 0.16% at the maximum. This gives rise to a 97% reduction in normalized transmitted power. Figure 3(b) shows the normalized transmittance $T$ and field enhancement factor (inset) at the maximum in time domain, as a function of the strength of the incident THz electric field. The strong transmission decrease of our system can be compared with previous works where the in-plane THz fields impinge on the graphene surface resulting in increased transmission [37,38]. To gain insights into the origin of the reduction in the normalized transmission through the angstrom gaps, we plot the maximum voltage across the gap, $V_{\text{gap,max}} = w \times E_{\text{gap,max}}$, driven by THz funneling [Fig. 3(c)] [22]. The dotted line indicates the case without nonlinearity, assuming the same field enhancement for all intensities. The measured data show that the voltage across the angstrom gap saturates at approximately 5 V. Intuitively, it is clear that the applied electric field is sufficiently strong to distort the quantum-mechanical barrier facilitating electron tunneling across the gap, making it more lossy, which in turn limits the field enhancement, and thereby $V_{\text{gap}}$ itself. This self-limited funneling can be observed without damage to the angstrom gaps because of the single-cycle nature of

transient THz waves [39,40] and the material robustness of graphene. We note that the subnanometer gap structure can be easily destroyed by an intense optical pulse because of its higher photon energy (~2 eV), so that the nonlinearity is much more difficult to observe before sample damage. Therefore, counterintuitively, given the same peak power, THz nonlinearity is much larger and much easier to observe than its optical counterpart.

We performed numerical calculations on the tunneling conductivity by assuming a square quantum barrier aided by an image potential [28]. In this approach, the electrical conductivity inside the gap under the bias voltage $V$ can be described with the tunneling current density $J$ as follows [22]:

$$\sigma = w\frac{J}{V}.$$

Regarding conductivity $\sigma$, a quantum-corrected plasmonic model provides dielectric constant $\varepsilon_{\mathrm{qc}}$ of the fictitious material inside the gap [29],

$$\varepsilon_{qc} = \varepsilon_{\infty} - \frac{\omega_g^2}{\omega\left(\omega + i\frac{\omega_g^2}{4\pi\sigma}\right)},$$

where $\varepsilon_{\infty}$ is the high frequency dielectric constant, $\omega_g$ the plasma frequency of the surrounding metal, and $\omega$ the frequency of the light fixed at 0.5 THz ($\lambda = 0.6$ mm) which is the center frequency of our spectrum. With the calculated $\varepsilon_{\mathrm{qc}}$, we obtain field enhancement both by analytical calculation based on the modal expansion [30] and by two-dimensional finite-difference time-domain (FDTD) simulation for a slit array structure. We note that the field enhancement factors obtained by these two calculations are remarkably close.

In Fig. 3(d), the calculated transmission $T/T_0$ is plotted as a function of the applied bias voltage $V$ for the effective gap size of $w = 3$ Å and permittivity of three [10,11], and the quantum barrier height of $\phi = 3$ eV. The dc applied bias voltages $V$ in the tunneling calculations are aligned with the measured voltages across the gap, $V_{\mathrm{gap,max}}$ for comparison. The fit (red line) is in good agreement with the experimental data denoted by red dots, reproducing the near-zero transmittance at high $V$, as well as the overall $V$dependence. In the inset of Fig. 3(d), we show the inverse of the total sum of the square of the difference between the calculation and the experimental data ${D_{\mathrm{total}}}^{-1}$ for various barrier heights $\phi$ and treating the width $w$ also as a variable [22]. It is noted that for the best fit, the barrier height and the barrier width need to fall around $\phi \sim 3$ eV and $w \sim 3$ Å. These values are consistent with the existing literature on the graphene gap width [11,35] and less than the accepted work function of Cu ($W_{\mathrm{Cu}} \sim 4.65$ eV), respectively. Figure 3(e) shows the potential barrier schematics of the Cu-SLG-Cu structure, using 7 eV of the Fermi level (Cu) and the applied bias of 0.005 V (top) and 5 V (bottom). FDTD results of the normalized intensity distribution for the low-intensity [0.005 V (top)] and the high-intensity [5 V (bottom)] cases, respectively, are consistent with experiments as shown in Fig. 3(f). The observed THz nonlinearity is thus well explained by the light-driven electron tunneling, which enhances the imaginary part of the effective dielectric constant of the angstrom gap. The tunneling-induced nonlinear response of the metallic gap can be much stronger at the long wavelength than near-infrared light, because of the mismatch between optical period and screening time. These strong nonlinearities at THz frequencies allow accurate determination of the quantum barrier height that is otherwise impossible.

In conclusion, we have demonstrated extreme terahertz nonlinearities of angstrom-size gaps fabricated by inserting a vertically oriented single layer graphene spacer between two coplanar copper films. This is achieved by intense terahertz funneling through the *infinitely* long angstrom gaps, across which a large transient potential difference facilitates electron tunneling. The tunneling electrons in turn change the effective index of refraction of the angstrom gaps, leading to the gigantic optical nonlinearity with a self-limiting nature. Background-free electromagnetic-manipulation of diverse chemical vapor deposition-compatible materials will enable linear and nonlinear angstrom optics in long wavelength domain, yielding invaluable information on the light matter interaction in quantum scale.

This work was supported by the National Research Foundation of Korea (NRF) Grant funded by the Korea government (MSIP) (CRI 2015031768, No. 2005-0093838, No. 2008-00580, No. 2011-0017494, WCI 2011-001) and the Brain Korea 21 Plus Project in 2014. This work was also partially supported by the Center for Advanced Meta-Materials (CAMM) funded by the Korea government (MSIP) as Global Frontier Project (CAMM-2014M3A6B3063709).

Y.-M. Bahk and B. J. Kang contributed equally to this work.

*rotermun@ajou.ac.kr
†dsk@phya.snu.ac.kr

[1] A. K. Geim and I. V. Grigorieva, Nature (London) **499**, 419 (2013).
[2] K. S. Novoselov, D. Jiang, F. Schedin, T. J. Booth, V. V. Khotkevich, S. V. Morozov, and A. K. Geim, Proc. Natl. Acad. Sci. U.S.A. **102**, 10451 (2005).
[3] S. J. Haigh, A. Gholinia, R. Jalil, S. Romani, L. Britnell, D. C. Elias, K. S. Novoselov, L. A. Ponomarenko, A. K. Geim, and R. Gorbachev, Nat. Mater. **11**, 764 (2012).
[4] F. Capasso, Science **235**, 172 (1987).
[5] G. Savini, A. C. Ferrari, and F. Giustino, Phys. Rev. Lett. **105**, 037002 (2010).
[6] R. Nandkishore, L. S. Levitov, and A. V. Chubukov, Nat. Phys. **8**, 158 (2012).
[7] G. Profeta, M. Calandra, and F. Mauri, Nat. Phys. **8**, 131 (2012).

[8] H. Min, R. Bistritzer, J.-J. Su, and A. H. MacDonald, Phys. Rev. B **78**, 121401 (2008).
[9] M. M. Fogler, L. V. Butov, and K. S. Novoselov, Nat. Commun. **5**, 4555 (2014).
[10] E. J. G. Santos and E. Kaxiras, Nano Lett. **13**, 898 (2013).
[11] J. Mertens *et al.*, Nano Lett. **13**, 5033 (2013).
[12] D. C. Marinica, A. K. Kazansky, P. Nordlander, J. Aizpurua, and A. G. Borisov, Nano Lett. **12**, 1333 (2012).
[13] C. Ciracì, R. T. Hill, J. J. Mock, Y. Urzhumov, A. I. Fernández-Domínguez, S. A. Maier, J. B. Pendry, A. Chilkoti, and D. R. Smith, Science **337**, 1072 (2012).
[14] K. J. Savage, M. M. Hawkeye, R. Esteban, A. G. Borisov, J. Aizpurua, and J. J. Baumberg, Nature (London) **491**, 574 (2012).
[15] H. Miyazaki and Y. Kurokawa, Phys. Rev. Lett. **96**, 097401 (2006).
[16] H.-T. Chen, W. J. Padilla, J. M. O. Zide, A. C. Gossard, A. J. Taylor, and R. D. Averitt, Nature (London) **444**, 597 (2006).
[17] M. A. Seo *et al.*, Nat. Photonics **3**, 152 (2009).
[18] J.-S. Huang *et al.*, Nat. Commun. **1**, 150 (2010).
[19] M. Schnell, P. Alonso Gonzalez, L. Arzubiaga, F. Casanova, L. E. Hueso, A. Chuvilin, and R. Hillenbrand, Nat. Photonics **5**, 283 (2011).
[20] M. Liu *et al.*, Nature (London) **487**, 345 (2012).
[21] K. Shibata, A. Umeno, K. M. Cha, and K. Hirakawa, Phys. Rev. Lett. **109**, 077401 (2012).
[22] See Supplemental Material at http://link.aps.org/supplemental/10.1103/PhysRevLett.115.125501 for a detailed discussion about experimental methods and theoretical calculation, which includes Refs. [23–30].
[23] D. Grischkowsky, S. Keiding, M. van Exter, and Ch Fattinger, J. Opt. Soc. Am. B **7**, 2006 (1990).
[24] P. C. M. Planken, H.-K. Nienhuys, H. J. Bakker, and T. Wenckebach, J. Opt. Soc. Am. B **18**, 313 (2001).
[25] Q. Wu and X.-C. Zhang, Appl. Phys. Lett. **67**, 3523 (1995).
[26] A. G. Stepanov, J. Kuhl, I. Kozma, E. Riedle, G. Almási, and J. Hebling, Opt. Express **13**, 5762 (2005).
[27] I. H. Baek, B. J. Kang, Y. U. Jeong, and F. Rotermund, J. Opt. Soc. Korea **18**, 60 (2014).
[28] J. G. Simmons, J. Appl. Phys. **34**, 1793 (1963).
[29] R. Esteban, A. G. Borisov, P. Nordlander, and J. Aizpurua, Nat. Commun. **3**, 825 (2012).
[30] F. J. Garcia-Vidal, L. Martin-Moreno, T. W. Ebbesen, and L. Kuipers, Rev. Mod. Phys. **82**, 729 (2010).
[31] J. S. Kyoung, M. A. Seo, H. R. Park, K. J. Ahn, and D. S. Kim, Opt. Commun. **283**, 4907 (2010).
[32] M. Shalaby *et al.*, Appl. Phys. Lett. **99**, 041110 (2011).
[33] A. Novitsky, M. Zalkovskij, R. Malureanu, and A. Lavrinenko, Opt. Commun. **284**, 5495 (2011).
[34] X. Chen *et al.*, Nat. Commun. **4**, 2361 (2013).
[35] A. V. Zaretski, B. C. Marin, H. Moetazedi, T. J. Dill, L. Jibril, C. Kong, A. R. Tao, and D. J. Lipomi, Nano Lett. **15**, 635 (2015).
[36] Y. Zhao, X. Li, Y. Du, G. Chen, Y. Qu, J. Jiang, and Y. Zhu, Nanoscale **6**, 11112 (2014).
[37] H. Y. Hwang, N. C. Brandt, H. Farhat, A. L. Hsu, J. Kong, and K. A. Nelson, J. Phys. Chem. B **117**, 15819 (2013).
[38] H. A. Hafez *et al.*, AIP Adv. **4**, 117118 (2014).
[39] O. Schubert *et al.*, Nat. Photonics **8**, 119 (2014).
[40] R. Huber, F. Tauser, A. Brodschelm, M. Bichler, G. Abstreiter, and A. Leitenstorfer, Nature (London) **414**, 286 (2001).